Orbit-lattice interaction and Jahn-Teller effect in the ^4E levels of Mn^{2+} in nearly tetrahedral clusters

C. Naud, C. Porte, F. Gendron, and R. Parrot

Université Pierre et Marie Curie, Laboratoire de Luminescence ,

Tour 13, 4 place Jussieu, 75230 Paris Cedex 05, France

(Received 2 November 1978)

The structure of the ^4E levels of Mn^{2+} in stressed ZnS and ZnSe crystals and in several organic compounds with distorted tetrahedral symmetry is investigated. First, the slight departure from tetrahedral symmetry of MnX_4 (X = S, Se, Cl, Br) molecular clusters is analyzed in terms of the normal coordinates $Q(E)$ and $Q(T_2)$ of a regular tetrahedron. Second, the influence of a linear coupling to E and T_2 strains and of a quadratic coupling to E strains is considered. Then, it is shown that for all clusters, the structure of the ^4E levels can most likely be interpreted in terms of an equivalent operator linear in $Q(E)$ and acting directly on the ^4E states. The values for the coupling parameters in the considered MnX_4 clusters are given and the origin of the equivalent operator is discussed. Finally, a study of the influence of the Jahn-Teller effect on the fine structure of the ^4E levels is made for all compounds. It is shown that the strength of the Jahn-Teller coupling to E vibrational modes is insufficient to drastically quench the influence of the T_2 strains on the observed vibronic ^4E states, the reduction parameters associated to these strains being greater than 0.35 for MnS_4 clusters and greater than 0.5 for the other clusters. This indicates that the electronic ^4E states are predominantly coupled to E strains, the electronic coupling to the T_2 strains being small or negligible.

I. INTRODUCTION

The analysis of the structure of the zero-phonon lines of the $^4T_1$, $^4T_2$ and ^4E levels of Mn^{2+} ions in cubic symmetry has attracted much attention in the past few years.[1-3] Although invoked for a long time,[1] a dynamical Jahn-Teller effect has been only recently observed and interpreted in the fluorescent $^4T_1$ level of Mn^{2+} in ZnS and ZnSe.[3] It was described by Ham's model[4] corresponding to a coupling to E vibrational modes. A dynamical Jahn-Teller effect has also been observed in the $^4T_2$ level at lower energy in these compounds[5]; in this case, it was shown that its main effect is to selectively transfer the intensity of the $^6A_1 \rightarrow \Gamma_8(\frac{3}{2})(^4T_2)$ transition to excited vibronic transitions. For these orbital triplets, the uniaxial-stress experiments indicate that the coupling to T_2 vibrational modes is either small or quenched by a Jahn-Teller coupling to E modes. In order to lift this ambiguity, Boccara[6] performed a linear dichroism experiment under uniaxial stresses. He concluded that the $^4T_2$ bands which are not subjected to a Jahn-Teller effect are almost insensitive to T_2 strains, while the $^4T_1$ bands are slightly coupled to T_2 strains. These results are in agreement with those obtained on the fundamental vibronic transitions $^6A_1 \rightarrow ^4T_2$ which are very weakly (or not) coupled to T_2 strains and only weakly coupled to E vibrational modes [the Huang-Rhys parameter being $S(^4T_2) = 0.6$ for ZnS:Mn and $S(^4T_2) = 1.2$ for ZnSe:Mn] so that the

influence of the T_2 strains is not strongly reduced by the Jahn-Teller effect. They are also in agreement with the results obtained on the fundamental vibronic states $^6A_1 \rightarrow ^4T_1$ for which the coupling to the T_2 strains is reduced by the Jahn-Teller coupling to E modes [the Huang-Rhys parameters being $S(^4T_1) = 1.8$ for ZnS:Mn and $S(^4T_1) = 2$ for ZnSe:Mn].

In an earlier paper on the ^4E level at lowest energy of Mn^{2+} in ZnS and ZnSe,[7] it was claimed that a coupling to E strains should be negligible, due to a third-order perturbation scheme in a theory restricted to the d^5 configuration. Therefore, the uniaxial-stress effects were tentatively interpreted in terms of a linear coupling to T_2 stress-induced strains via a second-order perturbation scheme involving the spin-orbit interaction and a stress-induced crystal-field Hamiltonian of T_2 symmetry.

However, optical experiments (reported in this paper) performed on the ^4E level at lower energy of Mn^{2+} ions in distorted tetrahedral molecular clusters, having shown splittings of the zero-phonon lines which could not be interpreted in terms of a coupling to T_2 intrinsic strains, led us to investigate the case of a linear coupling to E intrinsic strains and reconsider the nature of the coupling in stressed ZnS and ZnSe crystals.

As in the case of the orbital triplet levels the problems to be solved for the ^4E states of d^5 ions are (i) define the electronic structure of these states (of

course this problem will be more difficult to handle than in the case of orbital triplets whose electronic structure can be roughly defined in a d^5 configuration), and (ii) determine the nature of the vibronic interactions[8] and their influence on a ^4E state from a determination of the orbit-lattice coupling coefficients to E and/or T_2 strains.

In Sec. II, we describe the synthesis and the crystallographic structure of three organometallic compounds and we report their Raman spectra and the optical spectra for the ^4E bands. Several criteria governed the selection of organometallic compounds containing molecular clusters of the type MnX_4 ($X =$ Cl, Br, I). In order to avoid nonlinear coupling to instrinsic strains, we first selected clusters having distortions with respect to a regular tetrahedron corresponding to normal coordinates $Q(E)$ and $Q(T_2)$ of less than 0.1 Å. This limit corresponds to distortions which are roughly an order of magnitude greater than those appearing in highly stressed ZnS and ZnSe crystals. Then, we chose crystals showing well-defined EPR and Raman spectra and well-resolved optical spectra for the ^4E band.

Section III is devoted to a theoretical analysis of the coupling of a ^4E level to E and T_2 strains. This analysis, based mainly on the symmetry properties of several schemes restricted to the d^5 configuration, gives energy-level diagrams corresponding to a linear coupling to T_2 strains and a quadratic coupling to E strains. In particular, it is shown that a crystal-field model restricted to the d^5 configuration or a crude covalent model can give a linear coupling to E strains only by means of a third-order perturbation scheme. It is demonstrated that this analysis cannot account for all the observed structures of the ^4E levels.

In Sec. IV a phenomenological model based on the existence of an equivalent operator of E symmetry acting directly on the E level is presented. It is shown that this model is able to give a unified interpretation of all experimental results.

Finally, in Sec. V, we determine the orbit-lattice coupling coefficients (OLCC) for the compounds studied and discuss the influence of the Jahn-Teller effect on the fine structures of ^4E states.

II. EXPERIMENTS

A. Samples and apparatus

Amongst numerous organic crystals grown in the laboratory, we selected tetramethylammonium-tetrahalomanganate, whose chemical formula is $[(CH_3)_4N]_2Mn_xZn_{1-x}Cl_4$ with $x = 1$, 0.3, and 0.1. The synthesis of these crystals was performed following the method described by Cotton et al.[9] The sin-
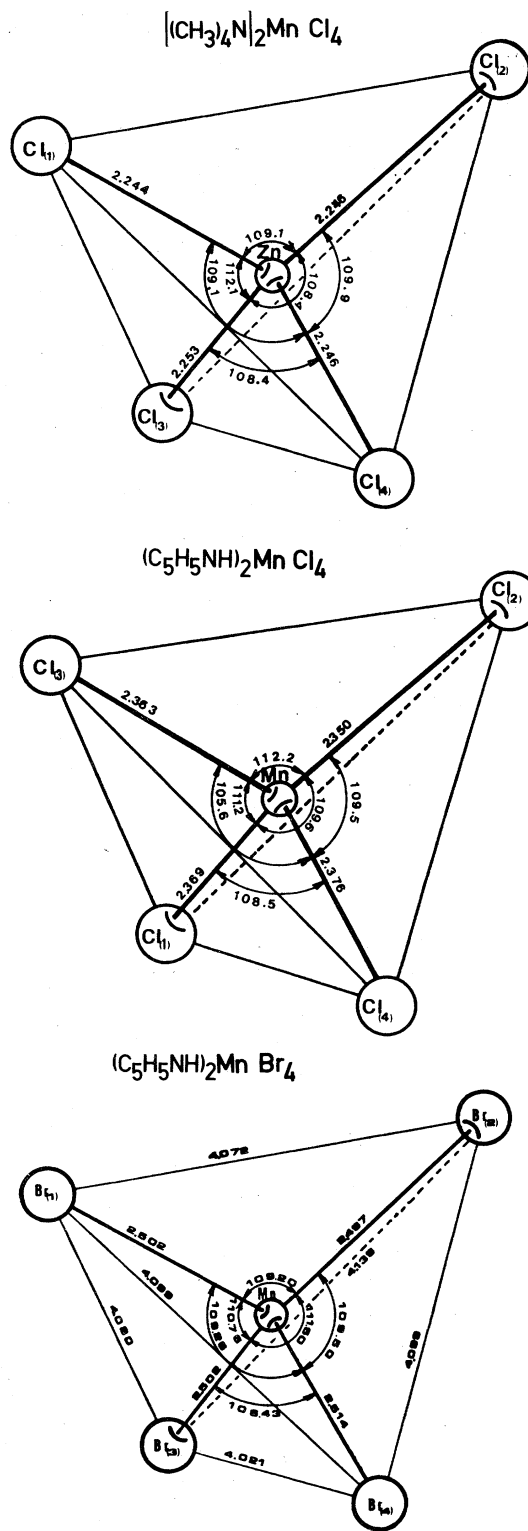

FIG. 1. Bond lengths and angles for the distorted MnX_4 clusters of $[(CH_3)_4N]_2MnCl_4$, $(C_5H_5NH)_2MnCl_4$, and $(C_5H_5NH)_2MnBr_4$.

gle crystals appear as platelets with dimensions of the order of $5 \times 5 \times 2$ mm^3. They are green yellow for $x = 1$ and 0.3 and colorless for $x \leq 0.1$. The crystals corresponding to $x = 0$ and 1 are isomorphic. The space group is D_{2h}^{16}, the dimensions of the unit cell being[10]: $a = 12.276$ Å, $b = 8.998$ Å, $c = 15.541$ Å for $x = 0$ and $a = 12.33$ Å, $b = 9.06$ Å, $c = 15.64$ Å for $x = 1$. For the molecular clusters $(MnCl_4)^{2-}$, the local symmetry is C_1 (see Fig. 1).

The other compounds are pyridinium-tetrahalomanganates II, whose chemical formula is $(C_5H_5NH)_2Mn_xZn_{1-x}X_4$ with $X = Cl,Br$ and $x = 1$, 0.3, and 0.1. These crystals were synthesized following the method of Cotton et al.[9] They appear as needles with dimensions of the order of $5 \times 2 \times 1$ mm^3. They are green for $x = 1$ and transparent for $x \leq 0.3$. The crystallographic data of Brassy et al.[11] show that the crystals with $X = Cl$ and Br are isostructural and triclinic. The space group is $P_{\bar{1}}$. The cell parameters are $a = 12.711$ Å, $b = 8.158$ Å, $c = 7.681$ Å, $\alpha = 100.38°$, $\beta = 93.43°$, and $\gamma = 88.78°$ for $(C_5H_5NH)_2MnCl_4$ and $a = 13.128$ Å, $b = 8.350$ Å, $c = 7.939$ Å, $\alpha = 100.61°$, $\beta = 96.66°$, and $\gamma = 87.63°$ for $(C_5H_5NH)_2MnBr_4$. The local symmetry for Mn^{2+} in the $(MnCl)_4^{2-}$ and $(MnBr_4)^{2-}$ clusters is C_1 (see Fig. 1).

The emission, absorption, and excitation experiments were performed at variable temperature between room temperature and 2.2 K with a Jobin-Yvon spectrometer HRS II. The irradiation of the crystals was performed either with a xenon lamp or an argon laser CR5 (coherent radiation).

The EPR spectra were obtained with a Varian E 2000 spectrometer operating at 35 GHz and a V 4502 Varian spectrometer operating at 10 GHz between room temperature and 2.2 K.

The Raman spectra were obtained with a Coderg PHO spectrometer equipped with a 1800-lines/mm grating. Helium neon and argon lasers from Spectra-physics were used for excitation.

B. Experiments

At 2.2 K, the emission spectra of the studied compounds consist of broad bands centered at 21 250 cm^{-1} for $[(CH_3)_4N]_2MnCl_4$, 19 200 cm^{-1} for $(C_5H_5NH)_2Mn_xZn_{1-x}Cl_4$, and 19 180 cm^{-1} for $(C_5H_5NH)_2Mn_xZn_{1-x}Br_4$. No zero-phonon line was observed in emission.

The absorption spectra were observed at 2.2 K in the range 2 500—8 000 Å for the crystals having the maximum concentration $(x = 1)$ in Mn^{2+}. The excitation spectra were obtained for all crystals described in Sec. II A; numerous narrow lines were observed at 2.2 K in the bands of Mn^{2+} appearing in the range 2 500—8 000 Å. However, except for the ^4E band it was not possible to unambiguously separate the

zero-phonon lines from the phonon-assisted lines the observed bands even with the aid of the Raman spectra. This was primarily due to the presence of low-energy phonons in the observed optical and Raman spectra. In particular, the fine-structure patterns for the zero-phonon lines of the $^6A_1 \rightarrow {}^4T_2$ transitions, which were expected to be composed of six lines in C_1 symmetry and to extend over approximately 100 cm^{-1}, were blurred by several phonon-assisted lines. (We did not try to recognize the lattice modes and the localized modes in the Raman spectra).

A part of the excitation spectrum and the Raman spectrum of $[(CH_3)_4N]_2MnCl_4$ are represented in Fig. 2. The inset gives the zero-phonon lines observed in mixed crystals $(x = 0.1)$. Four zero-phonon lines are easily distinguishable as well as a one phonon-assisted line appearing near 23 039 cm^{-1}.

Figure 3 corresponds to $(C_5H_5NH)_2Mn_{0.1}Zn_{0.9}Cl_4$. The excitation spectrum clearly shows two intense zero-phonon lines and phonon-assisted lines. The inset clearly shows two very weak lines appearing at 22 972 and 22 976 cm^{-1}. This structure was particularly difficult to be observed (slit: 0.2 cm^{-1}, $T = 2.2$ K, concentration $x = 0.1$).

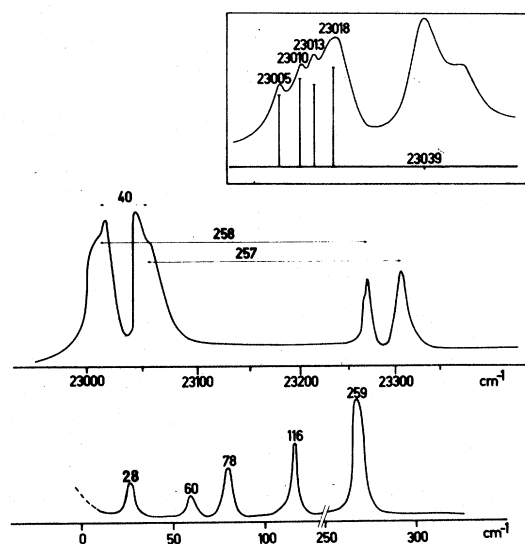In the case of $(C_5H_5NH)_2 Mn_{0.1}Zn_{0.9}Br_4$ (Fig. 4), four zero-phonon lines appear in the spectra. As in

FIG. 2. Excitation spectrum of the ^4E band and Raman spectrum (below) of $[(CH_3)_4N]_2MnCl_4$. The inset gives the details of the zero-phonon lines of the ^4E state obtained with a mixed crystals $[(CH_3)_4N]_2Mn_{0.1}Zn_{0.9}Cl_4$; the lines near 23 039 cm^{-1} are phonon-assisted lines; the vertical bars give the calculated energies and relative dipole strengths as calculated from the E-coupling model of Sec. IV.
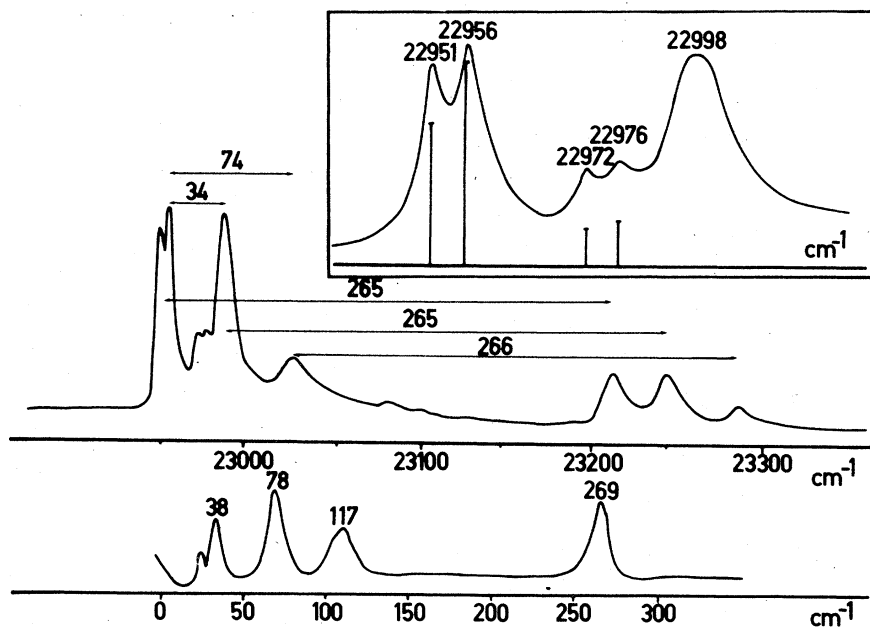
FIG. 3. Excitation spectrum of the ^4E band, Raman spectrum (below) and details of the zero-phonon lines (inset) for $(C_5H_5NH)_2Mn_{0.1}Zn_{0.9}Cl_4$.

the case of $(C_5H_5NH)_2Mn_{0.1}Zn_{0.9}Cl_4$ the two very weak zero-phonon lines appearing at 22 667 and 22 671 cm^{-1} were observed in selected single crystals showing well-defined EPR spectra.

For all compounds presented in Sec. II A, a study of the excitation spectra in terms of the concentration

$(x = 0.1, 0.3,$ and 1) only showed a broadening of all observed lines. This broadening rapidly obscures the fine structure observed in $[(CH_3)_4N]_2Mn_xZn_{1-x}X_4$, thus explaining the nonobservation of the structure of these lines in $[(CH_3)_4N]_2MnCl_4$ which was extensively studied by Vala et al.[12]
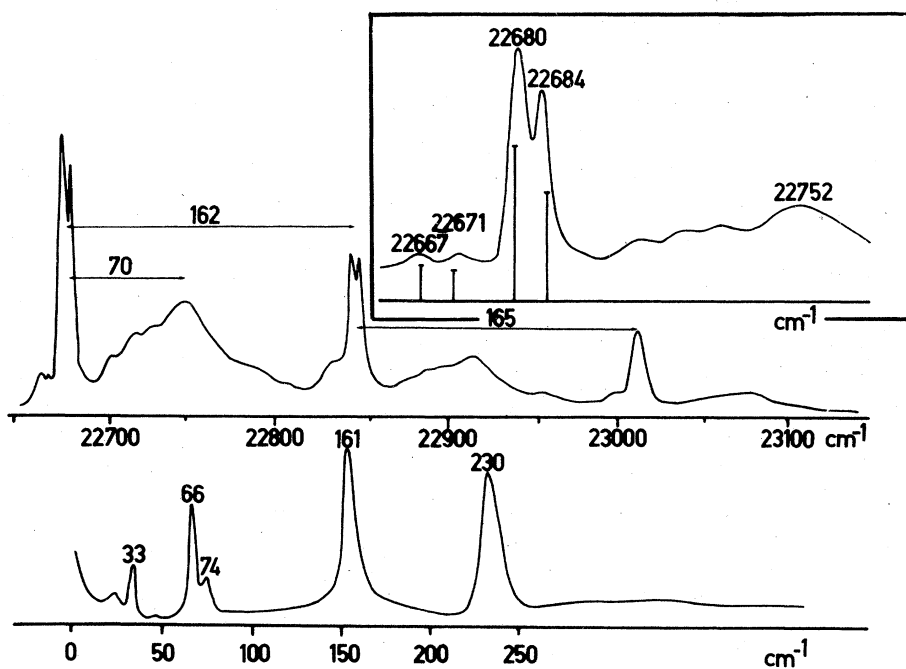

FIG. 4. Excitation spectrum of the ^4E band, Raman spectrum (below) and details of the zero-phonon lines (inset) for $(C_5H_5NH)_2Mn_{0.1}Zn_{0.9}Br_4$.

III. PRELIMINARY ASSUMPTIONS AND TENTATIVE MODELS

In the absence of a dynamic Jahn-Teller effect, the Hamiltonian governing the energy levels of d^5 ions in nearly cubic symmetry can be written

$$\mathcal{H} = \mathcal{H}_0 + \mathcal{H}_{cub} + \mathcal{H}_{SO} + \mathcal{H}_{SS} + \Delta\mathcal{H}_{strain} ,$$

where $\mathcal{H}_0$ and $\mathcal{H}_{cub}$ are, respectively, the free-ion Hamiltonian and the cubic part of the internal ligand field. $\mathcal{H}_{SO}$ is the spin-orbit interaction and $\mathcal{H}_{SS}$ is the spin-spin interaction. $\Delta\mathcal{H}_{strain}$ represents the noncubic part of the internal ligand field corresponding to stress-induced strains or intrinsic strains.

Our main assumption is that $\Delta\mathcal{H}_{strain}$ can be expanded in terms of a linear combination of normal coordinates $Q(\Gamma, M_\Gamma)$ transforming like the M_Γ component of a representation Γ of a cubic group. Explicitly, $\Delta\mathcal{H}_{strain}$ can be written

$$\Delta\mathcal{H}_{strain} = \sum_\Gamma \Delta\mathcal{H}(\Gamma) ,$$

with

$$\Delta\mathcal{H}(\Gamma) = eV(\Gamma) \sum_{M_\Gamma} \mathcal{E}(\Gamma, M_\Gamma) Q(\Gamma, M_\Gamma) ,$$

where the $\mathcal{E}$'s are electronic operators transforming like Γ, with M_Γ and the V's as the orbit-lattice coupling constants. (As indicated in Sec. I, this assumption is probably correct for the organic compounds studied in this paper).

A second assumption is that the electronic coupling between the studied $^4E(^5_vG)$ state and the $^4A_1(^5_vG)$ state is negligible in slightly distorted clusters (the spectroscopic terms are written as $^{2S+1}_vL$, v being the seniority number). This assumption is justified by the fact that there is no first-order coupling between these two states in cubic or nearly cubic symmetry allowed both by symmetry and seniority and that these states are nondegenerate. The energy difference $W(^4A_1) - W(^4E)$ can be easily deduced from the covalent model of Koide and Pryce[13] adapted to the case of a tetrahedral symmetry in Ref. 14. In this model the splitting of the $^4A_1(^5_vG)$ and $^4E(^5_vG)$ states is not due to a coupling between these states but to a coupling allowed by symmetry and seniority between the $^4E(^5_vD)$ and $^4E(^5_vG)$ states by the electrostatic interaction between electrons in σ orbitals. The net effect of this coupling is to shift the $^4A_1(^5_vG)$ states and the $^4E(^5_vG)$ states to lower energy when the covalency factor k increases, the shift being greater for the $^4E(^5_vG)$ state than for the $^4A_1(^5_vG)$ state.[14] If we admit for the energy of the ^5_vG state a value of 27 000

cm^{-1}, the covalency factors deduced from the observed energies of the centers of gravity of the $^4E(^5_vG)$ bands for the compounds studied are greater than $k = 0.95$, corresponding to a splitting of the $^4A_1$ and ^4E states greater than 700 cm^{-1}. (Following this assumption we will also neglect any vibronic coupling between the ^4E and $^4A_1$ states via E vibrational modes in Sec. V concerning the Jahn-Teller effect).

In order to determine the structure of a ^4E state in nearly cubic symmetry it is necessary to diagonalize simultaneously $\mathcal{H}_{SO} + \mathcal{H}_{SS} + \Delta\mathcal{H}_{strain}$. However before considering the influence of $\Delta\mathcal{H}_{strain}$ we will briefly recall the influence of $\mathcal{H}_{SO} + \mathcal{H}_{SS}$.

As previously demonstrated[7] the splitting of a ^4E level in cubic symmetry arises primarily from a second-order perturbation scheme involving the spin-orbit interaction. The energy levels are simply given by

$$W(t\tau) = \sum_{S'h'j'} \frac{|\langle ^4Et\tau|\mathcal{H}_{SO}|S'h'j't'\tau'\rangle|^2}{W(^4E) - W(^{2S'+1}h')} ,$$

with $t\tau = \Gamma_6$, Γ_7, or Γ_8. It can be easily found that the three fine-structure lines are equally spaced, with

$$W(\Gamma_6) - W(\Gamma_8) = W(\Gamma_8) - W(\Gamma_7)$$

and

$$W(\Gamma_6) - W(\Gamma_8) = \frac{1}{30}\{^4T_2\} + \frac{1}{30}\{^4T_1\} + \frac{1}{24}\{^2T_1\} + \frac{1}{24}\{^2T_2\} ,$$

the parameters $\{^{2S+1}h\}$ being defined by

$$\{^{2S+1}h\} = \sum_{h'} \frac{\langle ^4E\|\mathcal{H}_{SO}\|^{2S+1}h'\rangle\langle ^{2S+1}h'\|\mathcal{H}_{SO}\|^4E\rangle}{W(^4E) - W(^{2S+1}h')} .$$

The reduced matrix elements of $\mathcal{H}_{SO}$ are given by the general relation[15]

$$\langle Sh\|\mathcal{H}_{SO}\|S'h'\rangle = \langle Shjt\tau|\mathcal{H}_{SO}|S'h'j't'\tau'\rangle$$

$$\times \Omega_{jj'}^{-1}\begin{Bmatrix} S & S' & T_1 \\ h' & h & t \end{Bmatrix} .$$

As a typical example of this structure we can recall that of the ^4E level of Mn^{2+} in a cubic sites of ZnS.[7] In that case the calculated splitting $W(\Gamma_6) - W(\Gamma_8)$

$= 9.2$ cm^{-1} is in good agreement with the experimental value of 5 cm^{-1}. The contribution of the spin-spin interaction was found to be 2.6 cm^{-1}. The observed structure of the ^4E level of Mn^{2+} in the cubic sites of ZnS will be taken as a standard structure in tetrahedral clusters in the forthcoming computations.

In order to take into account simply of $\Delta\mathcal{H}_{strain}$ it is now necessary to restrict the problem to tetrahedral clusters. In T$_d$ symmetry $\Delta\mathcal{H}_{strain}$ reduces to

$$\Delta\mathcal{H}_{strain} = \Delta\mathcal{H}(A_1) + \Delta\mathcal{H}(E) + \Delta\mathcal{H}(T_2) \quad .$$

$$\Delta\mathcal{H}'(T_2) = \sum_{j\Gamma_i} \frac{\mathcal{H}_{SO}|^4\Gamma_i jt\,\tau\rangle \langle^4\Gamma_i jt\,\tau| \Delta\mathcal{H}(T_2) + \Delta\mathcal{H}(T_2)|^4\Gamma_i jt\,\tau\rangle \langle^4\Gamma_i jt\,\tau|\mathcal{H}_{SO}}{W(^4E) - W(^4\Gamma_i)} \quad ,$$

with $^4\Gamma_i \equiv {}^4T_{1i}, {}^4T_{2i}$ and

$$\Delta\mathcal{H}'(E^2) = \sum_{\tau} \frac{\Delta\mathcal{H}(E)|^4A_2 t\tau\rangle \langle^4A_2 t\tau| \Delta\mathcal{H}(E)}{W(^4E) - W(^4A_2)} \quad ,$$

with $t \equiv \Gamma_8$. The $^4A_2$ multiplet arises from the ^4_3F spectroscopic term.

The energy-level diagram corresponding to a linear coupling to T_2 strains via $\Delta\mathcal{H}'(T_2)$ is reported in Fig. 5 in terms of a parameter $\mathcal{R}(T_2)$ defined by

$$\mathcal{R}(T_2) = \sum_i \frac{\langle^4E \,||\mathcal{H}_{SO}||\,^4T_{2i}\rangle \langle^4T_{2i}\,||\Delta\mathcal{H}(T_2)||\,^4E\rangle}{W(^4E) - W(^4T_{2i})}$$

$$- \sum_j \frac{\langle^4E\,||\mathcal{H}_{SO}||\,^4T_{1j}\rangle \langle^4T_{1j}\,||\Delta\mathcal{H}(T_2)||\,^4E\rangle}{W(^4E) - W(^4T_{1j})} \quad .$$

The matrix elements of $\Delta\mathcal{H}'(T_2)$ and $\Delta\mathcal{H}'(E^2)$ were calculated in T_d^* from the complex tetragonal component system defined by Griffith.[15] Instead of writing numerous matrices or very large general formulas for the matrix elements in T_d^* we will only define unambiguously the reduced matrix elements of the spin-independent operators intervening in the relevant parameters. By slightly adapting Griffith's notations, the reduced matrix elements of $\Delta\mathcal{H}(\Gamma, M_\Gamma)$ are defined by T_d by

$$\langle Sh\,\theta|\Delta\mathcal{H}(\Gamma, M_\Gamma)|Sh'\theta'\rangle = [-1]^{h+\theta} V\begin{pmatrix} h & h' & \Gamma \\ -\theta & \theta' & M_\Gamma \end{pmatrix}$$

$$\times \langle Sh\,||\Delta\mathcal{H}(\Gamma)||\,Sh'\rangle \quad .$$

The reduced matrix elements of $\mathcal{H}_{SO}$ are defined above in T_d^*.

Figure 5 clearly shows that a linear coupling to T_2

It can be easily found from symmetry considerations, that a ^4E level could be coupled to the first-order to A_1 and E strains. However, in a pure d^5 configuration or when a mixing of the $^4E(^4_3D)$ and $^4E(^4_3G)$ is allowed by covalency, the first-order coupling to A_1 and E strains vanishes. Therefore we will first consider the higher-order perturbation schemes which allow a coupling to E and T_2 strains in the d^5 configuration. When restricted to this configuration, the second-order perturbation schemes predict a linear coupling to T_2 strains and a quadratic coupling to E strains. The relevant equivalent operators are

strains induces a splitting of the Γ_8 level linear in $\mathcal{R}(T_2)$. Furthermore, the energy differences $W(\Gamma_6) - W(\Gamma_8')$ and $W(\Gamma_8'') - W(\Gamma_7)$ increase with $\mathcal{R}(T_2)$. Obviously this model fails to give the energy levels of the ^4E state in $(C_5H_5NH)_2Mn_xZn_{1-x}Cl_4$ and $(C_5H_5NH)_2Mn_xZn_{1-x}Br_4$ but it could be correct in the case of $[(CH_3)_4N]_2Mn_xZn_{1-x}Cl_4$ (with $\mathcal{R}(T_2) \sim 40$ cm^{-1}). The case of the ^4E level of Mn^{2+} in ZnS will be considered in Sec. IV, where it will be shown that a linear coupling to E strains is in better agreement with experiments than a coupling to T_2 strains.

Figure 6 represents the energy-level diagram corresponding to a quadratic coupling to E strains.
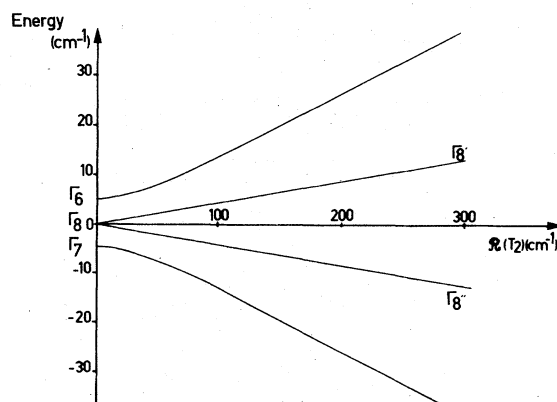
FIG. 5. Energy levels of a ^4E state in the case of a linear coupling to T_2 strains. $\mathcal{R}(T_2)$ is defined in Sec. III.
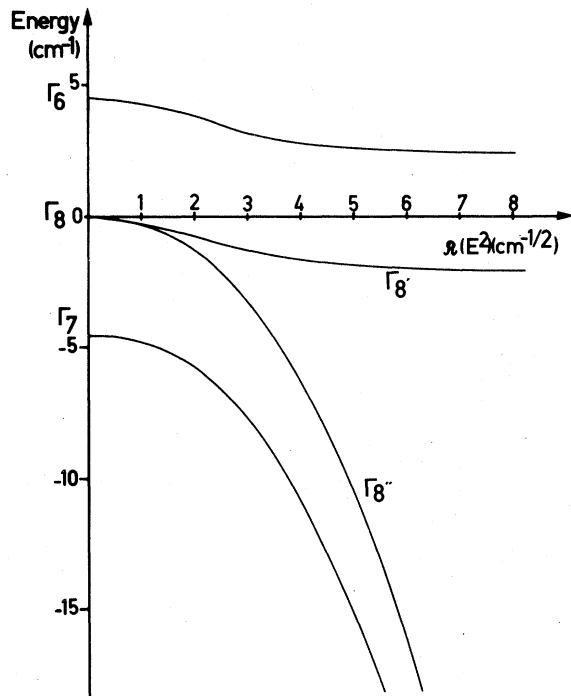
FIG. 6. Energy levels of a ^4E state in the case of a quadratic coupling to E strains. The quadratic shift common to all lines is represented. $\mathfrak{R}\,(E^2)$ is defined in Sec. III.

The parameter $\mathfrak{R}\,(E^2)$ is defined by

$$\mathfrak{R}^2(E^2) = \frac{|\langle\,^4E\,||\,\Delta\,\mathcal{3C}(E)\,||\,^4A_2\rangle|^2}{W(^4E) - W(^4A_2)} \; .$$

This figure shows that the energy levels are subjected to a common shift quadratic in $\mathfrak{R}(E^2)$ [and therefore quadratic in $Q(E)$]. However in this case, the energy differences $W(\Gamma_6) - W(\Gamma_8')$ and $W(\Gamma_8'') - W(\Gamma_7)$ remain constant when $\mathfrak{R}\,(E^2)$ increases. This model cannot account for the linear shift of the ^4E level of Mn^{2+} in ZnS in terms of the applied pressure $\vec{P}$ [see Fig. 7(a)] since this shift is obviously due to the stress-induced strains of A_1 symmetry while a quadratic coupling to E strains implies a shift quadratic in $\vec{P}$ superimposed to the linear shift due to A_1 strains. For $\vec{P}\,||\,[1\bar{1}0]$,

$$P = 16 \times 10^8 \text{ dyn/cm}^2 \; ,$$

the contribution of the quadratic shift should be 4 cm^{-1} and therefore easily observed. From a study of the intrinsic strains, it will be shown in Sec. V that a model linear in $Q(E)$ is more plausible for $MnCl_4$ and $MnBr_4$ clusters.

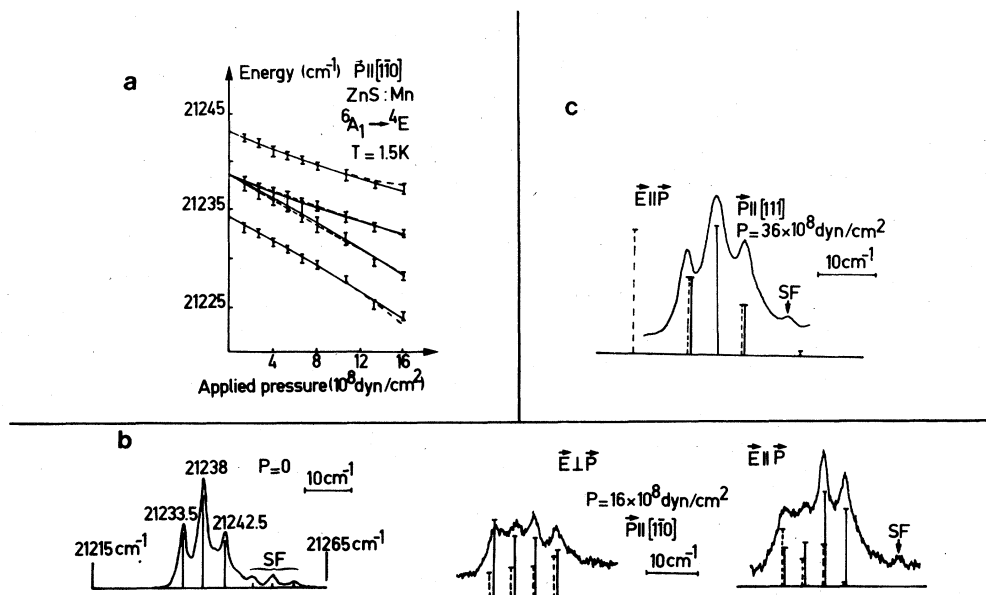A third-order perturbation scheme linear in the E strains was also considered. The corresponding

FIG. 7. Uniaxial-stress effects on ZnS:Mn. The dotted lines correspond to the model given in Ref. 7 (linear coupling to T_2 strains). The solid lines correspond to the E-coupling model as given in Sec. IV. SF corresponds to zero-phonon lines of axial Mn^{2+} centers in stacking faults.

operator is

$$\sum_{Jr_i,J'r_i'} \mathcal{3C}_{SO} |^4\Gamma_i Jt\tau\rangle \langle ^4\Gamma_i Jt\tau | \Delta\mathcal{3C}(E)|^4\Gamma_i'J't'\tau'\rangle \langle ^4\Gamma_i'J't'\tau' | \mathcal{3C}_{SO} \frac{1}{[W(^4E) - W(^4\Gamma_i)][W(^4E) - W(^4\Gamma_i')]} .$$

A numerical calculation shows that the contribution of this scheme is negligible with respect to the contribution of the previous scheme linear in the T_2 strains. (For example, it predicts a splitting of the Γ_8 state less than 50 cm^{-1} per unit E strain in the case of ZnS:Mn.)

IV. E-COUPLING MODEL

A. Energy levels

Since none of the above models permits a unified interpretation of the observed structures, we will now formally consider the case of a linear coupling to E strains by means of an equivalent operator $\Delta\mathcal{3C}'(E)$ acting to the first order on a ^4E state. Such an operator does not exist in a d^5 configuration, but it appears when configuration interactions or covalency are taken into account (Appendix A).

The energy-level diagram corresponding to a linear coupling to E strains is given in Fig. 8 in terms of a parameter $\mathcal{R}(E)$ defined by

$$\mathcal{R}(E) = \langle E_\alpha | \Delta\mathcal{3C}(E_\gamma) | E_\beta \rangle V^{-1} \begin{bmatrix} E & E & E \\ \alpha & \beta & \gamma \end{bmatrix} .$$

This figure clearly shows that the E-coupling model provides a unified interpretation of the energy-level diagrams for all considered cases. However, we must remark that for $[(CH_3)_4N]_2Mn_xZn_{1-x}Cl_4$, a linear
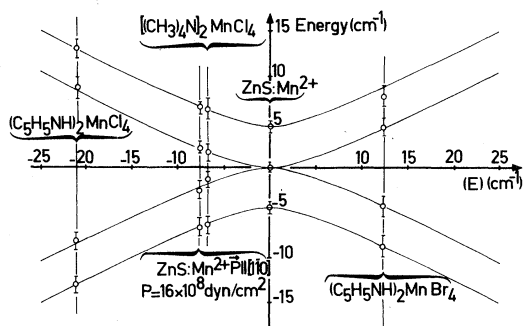

FIG. 8. Energy levels of a ^4E state in the case of a linear coupling to E strains. $\mathcal{R}(E)$ is defined in Sec. IV. The points correspond to the observed energy levels in the organic compounds and in ZnS for $P = 0$ and $P = 16 \times 10^8$ dyn/cm^2 ($\vec{P} \| [1\bar{1}0]$). The numerical values for $\mathcal{R}(E)$ are given in Table I.

coupling to T_2 strains is equally valid (see Sec. III B) and that the experimental results do not permit determining unambiguously the nature of the coupling in that case. For ZnS, the hypothesis of a preponderant linear coupling to E strains is more justified than the previous hypothesis[7] of a linear coupling to T_2 strains for interpreting all uniaxial stress experiments. More precisely, for an applied pressure parallel to a $[1\bar{1}0]$ axis, the shifts and splittings of the fine-structure lines can be fitted equally well either with $\mathcal{R}(T_2) = -40$ cm^{-1} (for $P = 16 \times 10^8$ dyn/cm^2) or $\mathcal{R}(E) = -7.6$ cm^{-1} (for $P = 16 \times 10^8$ dyn/cm^2) as shown in Fig. 8. But for $\vec{P} \| [111]$, the E-coupling model which predicts no effect on the fine-structure lines [since $Q(E) = 0$] is in agreement with the experimental results while a linear coupling to T_2 strains predicts relatively large shifts and splittings [see Fig. 7(c)].

Although in ZnSe the experimental results[16] are less precise than in ZnS, the absence of a splitting of the $^6A_1 \rightarrow \Gamma_8$ transition for $\vec{P} \| [111]$ is an argument in favor of the E-coupling model.

B. Strains and dipole strengths

The bond lengths and angles defining the molecular clusters in organic compounds are given in Fig. 1. The relevant normal coordinates[17] and their amplitudes are given in Table I. We must note that the precision of the calculation of the normal coordinates is strongly limited by the precision of the crystallographic data for the organic compounds ($\Delta Q \sim \pm 0.01$ Å)

The relative dipole strengths (RDS) of the zero-phonon transitions were calculated from the general formula

$$(^6A_1 \rightarrow ^4Ef) = \frac{1}{N^2} \sum_{t\tau(^6A_1)} \left| \sum_{t'\tau'(^4E)} \langle ^6A_1 t\tau | \mathcal{3C}_{SO} |^4T_1 t\tau\rangle \right.$$
$$\left. \times \langle ^4T_1 t\tau | \mathcal{3C}_{equ.}(T_2) |^4Et'\tau'\rangle \langle ^4Et'\tau' |^4Ef\rangle \right|^2 ,$$

where $\mathcal{3C}_{equ.}(T_2)$ is an equivalent operator due to the composition of the electric-dipole moment with the odd part of the ligand field.[5] The perturbed ^4E states are defined in terms of the projector $\langle ^4Et'\tau' |^4Ef\rangle$ on cubic $|^4Et'\tau'\rangle$ states.

Very tedious calculations involving values of the normal coordinates $Q(E_\theta)$, and $Q(E_\epsilon)$, the orienta-

TABLE I. Normal coordinates associated to the molecular clusters defined in Fig. 1 and to MnS_4 clusters in stressed ZnS, and orbit-lattice coupling constants V. $\mathfrak{R}(E)$ is defined in Sec. IV A.

	ZnS:Mn $\vec{P} \parallel [1\bar{1}0]$ $P = 16 \times 10^8$ dyn/cm^2	$[(CH_3)_4N]_2Mn\,Cl_4$	$(C_5H_5NH)_2MnCl_4$	$(C_5H_5NH)_2MnBr_4$
$Q(E_\theta)$ (Å)	0.004	0.030	0.073	0.077
$Q(E_\epsilon)$ (Å)	0	−0.052	0.001	0.005
$[Q^2(E_\theta) + Q^2(E_\epsilon)]^{1/2}$	0.004	0.060	0.073	0.077
$[Q^2(T_{2a\xi}) + Q^2(T_{2a\eta}) + Q^2(T_{2a\zeta})]^{1/2}$	0.006	0.006	0.020	0.012
$[Q^2(T_{2b\xi}) + Q^2(T_{2b\eta}) + Q^2(T_{2b\zeta})]^{1/2}$	0.004	0.050	0.120	0.085
$\mathfrak{R}(E)$ (cm^{-1})	−7.6	−6.7	−21	12.4
V (cm^{-1}/Å)	−870	−55	−140	80

tion of the clusters with respect to the growing planes of the crystals, and the orientation of the electric field of the light, permitted us to calculate the RDS given in Figs. 2, 3, 4, and 7. We must note that the calculated RDS's for the organic compounds are in excellent agreement with the experiments, thus justifying again the E-coupling model.

V. JAHN-TELLER EFFECT AND ORBIT LATTICE INTERACTION IN THE MOLECULAR-CLUSTER MODEL

A. Jahn-Teller effect

To account for a linear Jahn-Teller effect on an orbital doublet in cubic symmetry is necessary to add to the classical Hamiltonian given in Sec. III the vibronic Hamiltonian

$$\mathcal{H}_v = \mathcal{H}_{el} + \mathcal{H}_K + \mathcal{H}_{JT} \ ,$$

where $\mathcal{H}_{el}$ and $\mathcal{H}_K$ are, respectively, the elastic and kinetic energy associated to an effective vibrational mode $Q_{v\theta}, Q_{v\epsilon}$ belonging to E. $\mathcal{H}_{JT}$ is the interaction Hamiltonian given by

$$\mathcal{H}_{JT} = V(\mathcal{E}_\theta Q_{v\theta} + \mathcal{E}_\epsilon Q_{v\epsilon}) \ ,$$

where V represents the strength of the Jahn-Teller coupling and the $\mathcal{E}$'s are the electronic operators defined in Ref. 8.

The influence of $\mathcal{H}_v$ on E states having been extensively studied, we will briefly recall the main results of the theory.[8]

First, the matrix elements of orbital operators acting directly on the fundamental vibronic states of an orbital doublet are identical to the matrix elements of reduced orbital operators, acting on the electronic doublet, the reduction factors being p and q for A_2 and E operators, respectively. Approximate expres-

sions for p and q which are sufficient for our purpose are

$$p = \exp(-1.974 S^{0.761}) \ ,$$

where $S = E_{JT}/\hbar\omega$ and $0.1 < S < 3$ and $q = \frac{1}{2}(1 + p)$ (q is at most $\cong \frac{1}{2}$ for $E_{JT} \gg \hbar\omega$, see Fig. 9). E_{JT} is related to V and to the angular frequency ω of the effective phonon by $E_{JT} = V^2/2\mu\omega^2$, μ being the mass of the effective phonon.

Second, in a second-order perturbation scheme involving different electronic states, the orbital parts of the matrix elements which belong to A_2 and E are reduced by p and q, respectively.

From the above results it can be shown that the main operators which intervene in the E-coupling model are reduced. Obviously, the operator $\Delta\mathcal{H}'(E)$
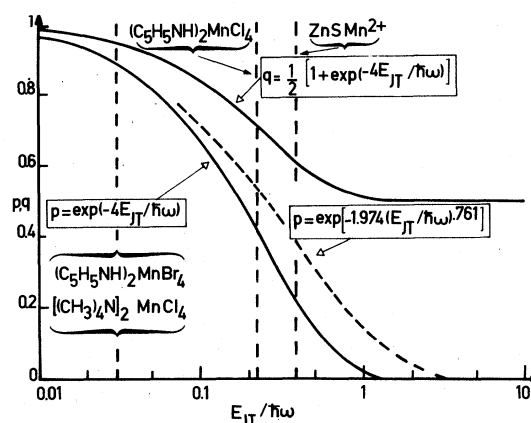

FIG. 9. Upper limit for the Huang-Rhys parameter $S = E_{JT}/\hbar\omega$ and for the reduction factors p, q, for the MnS_4, $MnCl_4$, and $MnBr_4$ clusters. The energies of the effective vibrational modes are chosen to be 100 cm^{-1} for MnS_4 clusters in ZnS (see Refs. 5, 18, 19) and 35 cm^{-1} for the other clusters.

defined in Sec. IV E is reduced by a factor q (we neglect a second-order interaction involving the excited vibronic levels of the ^4E state[8]). The second-order contribution of the spin-orbit interaction is, at most, reduced by the factor q. (The method used to obtain the symmetry of the orbital part of $\mathcal{H}_{SO}^2$ is a simple extension of that presented in Appendix B; it shows that the orbital part of $\mathcal{H}_{SO}^2$ acting on a ^4E state spans the A_1 and E representations of T_d). In order to find the reduction factor associated to T_2 strains, we have to consider the perturbation equivalent operator $\Delta\mathcal{H}'(T_2)$ defined in Sec. III. As shown in Appendix B, the orbital part of this operator belongs to A_2, therefore the reduction factor associated to T_2 strains is p. This means that a strong coupling to E vibrational modes can completely quench the influence of T_2 strains on a E state.

Coming back to the interpretation of our experimental results, it will be shown that the Jahn-Teller coupling to E modes is not strong enough to completely quench the influence of T_2 strains on E states, thus indicating that the electronic ^4E states of Mn^{2+} in the considered clusters are only weakly coupled to T_2 strains. The following demonstration is based on the determination of the orbit-lattice coupling coefficients in the molecular cluster approximation.

First, the OLCC's $V(E)$ are defined in terms of $\mathcal{R}(E)$ by

$$V(E) = \tfrac{1}{2}\mathcal{R}(E)[Q^2(E_\theta) + Q^2(E_\epsilon)]^{-1/2} ,$$

(the factor $\tfrac{1}{2}$ permits defining OLCC's analogous to those of Ham[8]). They are given in Table I. Second, an upper limit for the Huang-Rhys parameter S (and for the reduction parameters p and q) has been calculated for each cluster, following Ham's cluster model. In order to obtain an upper limit for S $[S = V^2(E)/2\mu\hbar\omega^3]$, a very low energy for the effective phonons of E symmetry was chosen for the MnX_4 clusters in organic compounds. The results are summarized in Fig. 9. For $MnCl_4$ and $MnBr_4$ clusters, the reduction factors p and q are greater than 0.5. For the MnS_4 clusters they are greater than 0.35.

VI. CONCLUSION

Very detailed experimental and theoretical studies of the fine-structure lines of a ^4E state of Mn^{2+} in distorted tetrahedral clusters have shown that electronic models restricted to the d^5 configuration give unreliable indications concerning the strain effects on the orbital doublets of d^5 ions.

In order to describe the unusual structure of ^4E states of d^5 ions, a phenomenological model based on symmetry considerations only has been elaborated which accounts for the observed vibronic structure of the ^4E states in terms of a coupling to E strains. In a

second step, Ham's cluster model for vibronic interactions has been considered in order to choose between the two following hypotheses which can account for the nonobservation of a coupling to the relatively large T_2 strains existing in the distorted clusters: (i) the electronic ^4E states are coupled both to E and T_2 strains, but the effect of the coupling to T_2 strains is quenched by a strong Jahn-Teller coupling to E vibrational modes, or (ii) the electronic ^4E states are predominantly coupled to E strains, the electronic coupling to T_2 strains being small or negligible. Although probably very crude (as previously shown in the case of the triplet states of Mn^{2+} in stressed ZnS and ZnSe), Ham's cluster model indicates that the coupling to E vibrational modes is small so that hypothesis (ii) must be retained.

Finally, several perturbation schemes contributing to the E-coupling model have been considered. However, a theory showing clearly the preponderance of the electronic coupling to E strains remains to be elaborated from a detailed comparison of the various perturbation schemes contributing to the coupling to E and T_2 strains.

ACKNOWLEDGMENTS

APPENDIX A

A perturbation equivalent operator of E symmetry acting to the first order on ^4E states can be obtained, *in the case of a tetrahedral symmetry*, from a second-order perturbation scheme involving the odd part of the cubic field and the odd part of the intrinsic or stress-induced strains. The relevant operator can be written

$$\Delta\mathcal{H}(E) = 2\sum_{^4E_{odd}} \frac{\mathcal{H}_{odd}(A_1)|^4E_{odd}\rangle\langle^4E_{odd}|\Delta\mathcal{H}_{odd}(E)}{W(^4E) - W(^4E_{odd})} ,$$

a $\mathcal{H}_{odd}(A_1)$ being the odd part of the cubic field defined in terms of spherical harmonics Y_ℓ^q by

$$\mathcal{H}_{odd}(A_1) = \sum_{\substack{k=3,7 \\ q}} A_k^q \langle r^k \rangle Y_k^q ,$$

and $\Delta\mathcal{3C}_{odd}(E)$ being the odd part of the crystal field of E symmetry defined by

$$\Delta\mathcal{3C}_{odd}(E) = \sum_{\substack{k=5,7 \\ q}} A_k^q \langle r^k \rangle Y_k^q \ .$$

For d^5 ions, the relevant intermediate states $|^4E_{odd}\rangle$ must be chosen in the $3d^4nl$ configurations with $l \geqslant 3$. In the case of the $3d^44f$ configuration, the $|^4E_{odd}\rangle$ states should be constructed from the multiplets ^4D, ^4G, ^4H, ^4I, and ^4J (the parent multiplets of d^4 being ^3H and ^3G) ^4D, ^4G, ^4H, and ^4I (the parent multiplet being $^3F_2$), and ^4D, ^4G, ^4H (the parent multiplets being ^3D and ^5D). A detailed calculation of the amplitude of $\Delta\mathcal{3C}(E)$ being out of the scope of this paper, we will only give a very crude value of the contribution of $\Delta\mathcal{3C}(E)$ to the parameter $\mathcal{R}(E)$ defined in Sec. IV. By taking $\mathcal{3C}_{odd}(A_1) = 10^4 \ cm^{-1}$, $\Delta\mathcal{3C}_{odd}(E) = 20 \ cm^{-1}$, this value corresponds to

$$[Q^2(E_\theta) + Q^2(E_\varepsilon)]^{1/2} = 0.1 \ \text{Å}$$

and

$$W(^4E) - W(^4E_{odd}) \simeq W(3d^5) - W(3d^44f) = -2 \times 10^5 \ cm^{-1} \ ;$$

we get an upper limit for $\mathcal{R}(E)$ of the order of $1 \ cm^{-1}$.

Of course, third-order perturbation schemes also contribute to the equivalent operator of E symmetry. We can consider, for example, the equivalent operator

$$\Delta\mathcal{3C}'(E) = \sum_{^4E_{odd} \ ^4E'_{odd}} \frac{\mathcal{3C}_{odd}(A_1) |^4E_{odd}\rangle \ \langle^4E_{odd}|\Delta\mathcal{3C}_{even}(E)|^4E'_{odd}\rangle \ \langle^4E'_{odd}|\mathcal{3C}_{odd}(A_1)}{[W(^4E) - W(^4E_{odd})][W(^4E) - W(^4E'_{odd})]} \ ,$$

where $\Delta\mathcal{3C}_{even}(E)$ is the even part of the crystal field of E symmetry. The relevant intermediate states belong to the $3d^4nl$ configuration with $l \geqslant 1$.

By taking

$$\mathcal{3C}_{odd}(A_1) = 10^4 \ cm^{-1} \ , \ \ \Delta\mathcal{3C}_{even}(E) = 400 \ cm^{-1}$$

(for $Q(E) = 0.1 \ \text{Å}$) and

$$W(3d^5) - W(3d^44p) = -8 \times 10^4 \ cm^{-1}$$

we get a contribution of the order of $6 \ cm^{-1}$.

APPENDIX B:

In a second-order perturbation scheme via the spin-orbit interaction $\mathcal{3C}_{SO}$ and a spin-independent operator of the form $Q(\Gamma, M_\Gamma)\mathcal{E}(\Gamma, M_\Gamma)$, the matrix elements to consider are

$$M(ShMM'\theta\theta'') = \sum_{h'\theta'} (\langle ShM\theta|\mathcal{3C}_{SO}|Sh'M'\theta'\rangle \ \langle Sh'M'\theta'|Q(\Gamma, M_\Gamma)\mathcal{E}(\Gamma, M_\Gamma)|ShM'\theta''\rangle$$

$$+ \langle ShM\theta|Q(\Gamma, M_\Gamma)\mathcal{E}(\Gamma, M_\Gamma)|Sh'M\theta'\rangle \ \langle Sh'M\theta'|\mathcal{3C}_{SO}|ShM'\theta''\rangle) \frac{1}{W(Sh) - W(Sh')} \ .$$

In a cubic group, these matrix elements can be expanded as

$$M(ShMM'\theta\theta'') = \sum_{h'\theta'j\Gamma M_\Gamma} \frac{\langle Sh \|\mathcal{3C}_{SO}\| Sh'\rangle \ \langle h' \|\mathcal{E}(\Gamma)\| h\rangle}{W(Sh) - W(Sh')} (-1)^{1+J+S-M}[-1]^{h+\theta+h'+\theta'}$$

$$\times \left[V\begin{pmatrix} h & h' & T_1 \\ -\theta & \theta' & j \end{pmatrix} V\begin{pmatrix} h' & h & \Gamma \\ -\theta' & \theta'' & M_\Gamma \end{pmatrix} + \eta[-1]^\Gamma V\begin{pmatrix} h & h' & \Gamma \\ -\theta & \theta' & M_\Gamma \end{pmatrix} V\begin{pmatrix} h' & h & T_1 \\ -\theta' & \theta'' & j \end{pmatrix} \right] \begin{pmatrix} S & 1 & S' \\ -M & -j & M' \end{pmatrix} Q(\Gamma, M_\Gamma) \ ,$$

where $\langle Sh \|\mathcal{3C}_{SO}\| Sh'\rangle$ is the reduced matrix element of $\mathcal{3C}_{SO}$. The coupling coefficients refer to the complex tetragonal component system defined by Griffith,[15] therefore $j = -1, 0, +1$. η is defined by

$$\overline{\langle h \|\mathcal{E}(\Gamma)\| h'\rangle} = \eta \langle h \| \mathcal{E}(\Gamma) \| h'\rangle \ .$$

The summation on θ' can now be easily performed by reordering the elements of the V's and using the following

general equation for a complex component system:

$$\sum_{\Phi^\dagger} [-1]^{f+\Phi^\dagger} V \begin{bmatrix} a & e & f \\ \alpha^\dagger & \epsilon^\dagger & \Phi^\dagger \end{bmatrix} V \begin{bmatrix} b & f & d \\ \beta^\dagger & -\Phi^\dagger & \delta^\dagger \end{bmatrix} = \sum_{c\gamma^\dagger} \lambda(c)[-1]^{c+\gamma^\dagger} W \begin{bmatrix} a & b & c \\ d & e & f \end{bmatrix} V \begin{bmatrix} a & b & c \\ \alpha^\dagger & \beta^\dagger & \gamma^\dagger \end{bmatrix} V \begin{bmatrix} c & d & e \\ -\gamma^\dagger & \delta^\dagger & \epsilon^\dagger \end{bmatrix} .$$

[For a real component system see Eq. (4.11) of Ref. 15.] A straightforward calculation gives

$$M(ShMM'\theta\theta'') = \sum_{c\gamma h'j\Gamma M_\Gamma} \frac{\langle Sh \| \mathcal{K}_{SO} \| Sh' \rangle \langle h' \| \mathcal{S}(\Gamma) \| h \rangle}{W(Sh) - W(Sh')} \lambda(c) W \begin{bmatrix} T_1 & \Gamma & c \\ h & h & h' \end{bmatrix} (-1)^{1+J+S-M}[-1]^{h+\theta+c+\gamma}$$

$$\times [1 + \eta(-1)^{T_1+c}] V \begin{bmatrix} T_1 & \Gamma & c \\ j & M_\Gamma & \gamma \end{bmatrix} \begin{bmatrix} S & 1 & S \\ -M & -j & M' \end{bmatrix} Q(\Gamma, M_\Gamma) V \begin{bmatrix} h & h & c \\ \theta'' & -\theta & -\gamma \end{bmatrix} .$$

This general formula clearly shows that the orbital part of the matrix elements spans the representations c of a cubic group (see the last V symbol). It also permits a straightforward calculation of the amplitudes of the orbital operators spanning the representations c.

The particular case considered in Sec. V corresponds to $\Gamma = T_2$, $h = E$. The strongest selection rule is given by the factor $1 + \eta(-1)^{T_1+c}$ which is nonzero only when $c = A_2$.

[1] A. Landi, C. Blanchard, and R. Parrot, Phys. Lett. A **36**, 267 (1971).

[2] M. Y. Chen, D. S. McClure, and E. I. Solomon, Phys. Rev. B **6**, 1690 (1972); **6**, 1697 (1972); **9**, 4690 (1974).

[3] R. Parrot, C. Naud, C. Porte, D. Fournier, A. C. Boccara, and J. C. Rivoal, Phys. Rev. **17**, 1057 (1978).

[4] F. S. Ham, Phys. Rev. **138**, A1727 (1965).

[5] R. Parrot, C. Naud, and F. Gendron, Phys. Rev. B **13**, 3748 (1976).

[6] A. C. Boccara (private communication).

[7] R. Parrot and C. Blanchard, Phys. Rev. **6**, 3992 (1972).

[8] F. S. Ham, Phys. Rev. **166**, 307 (1968).

[9] F. A. Cotton, D. Goodgame, and M. Goodgame, J. Am. Chem. Soc. **84**, 167 (1962).

[10] J. R. Wiesner, R. C. Srivastava, C. H. L. Kennard, M. Di-Vaira, and E. C. Lingafelter, Acta Crystallogra. **23**, 565 (1967).

[11] C. Brassy, R. Robert, B. Bachet, and R. Chevalier, Acta Crystallogra. Sect. B **32**, 1371 (1976).

[12] M. T. Vala, C. J. Ballhausen, R. Dingle, and S. L. Holt, Mol. Phys. **23**, 217 (1972).

[13] S. Koide and M. H. L. Pryce, Philos. Mag. **3**, 607 (1958).

[14] C. Blanchard and R. Parrot, Solid State Commun. **10**, 413 (1972).

[15] J. S. Griffith, *The Irreducible Tensor Method for Molecular Symmetry Groups* (Prentice-Hall, Englewood Cliffs, 1962).

[16] C. Blanchard, A. Landi, C. Naud, and R. Romestain, Phys. Lett. A **44**, 17 (1973).

[17] For the definition of the normal coordinates, see M. D. Sturge, in *Solid State Physics,* edited by F. Seitz and G. Turnbull (Academic, New York, 1967), Vol. 20.

[18] F. S. Ham and G. A. Slack, Phys. Rev. **4**, 777 (1971).

[19] J. T. Vallin and G. D. Watkins, Phys. Rev. B **9**, 2051 (1974).